Observations of Aerosol-Vapor Pressure Deficit-Evaporative Fraction coupling over India

Chandan Sarangi[1,2,7*], Tirthankar Chakraborty[3,4], Sachchidanand Tripathi[1,3*], Mithun Krishnan[1], Ross Morrison[5], Jonathan Evans[5], Lina Mercado [5,6]

Affiliations:

[1] Department of Civil engineering, Indian Institute of Technology, Kanpur, Kanpur, India

[2] Department of Civil engineering, Indian Institute of Technology, Madras, Chennai, India

[3] Center for Environmental Science and Engineering, Indian Institute of Technology, Kanpur

[4] School of the Environment, Yale University

[5] UK Centre for Ecology & Hydrology, Wallingford, UK

[6] Department of Geography, University of Exeter, UK

[7] Laboratory of Atmospheric and Climate Sciences, Indian Institute of Technology, Madras, Chennai, India

* Corresponding authors: snt@iitk.ac.in and chandansarangi@iitm.ac.in

Abstract

North India is a densely populated subtropical region with heavy aerosol loading (mean Aerosol Optical Depth or AOD ~ 0.7), frequent heatwaves and strong atmosphere-biosphere coupling, making it ideal for studying the impacts of aerosols and temperature variation on latent heat flux (LH) and evaporative fraction (EF). Here, using in situ observations during the onset of the summer monsoon over a semi-natural grassland site in this region, we confirm that strong co-variability exists among aerosols, LH, air temperature (T_{air}) and vapor pressure deficit (VPD). Since the surface evapotranspiration is strongly controlled by both physical (available energy and moisture demand) and physiological (canopy and aerodynamic resistance) factors, we separately analyze our data for different combinations of aerosols and T_{air}/VPD changes. We find that aerosol loading and warmer conditions both reduces SH. Further, we find that an increase in atmospheric VPD, tends to decrease the gross primary production (GPP) and thus LH, most likely as a response to stomatal closure of the dominant grasses at this location. In contrast, under

heavy aerosol loading, LH is enhanced partly due to the physiological control exerted by the diffuse radiation fertilization effect (thus increasing EF). Moreover, LH and EF increases with aerosol loading even under heatwave conditions, indicating a decoupling of plant's response to VPD enhancement (stomatal closure) in presence of high aerosol conditions. Our results encourage detailed in situ experiments and mechanistic modelling of AOD-VPD-EF coupling for better understanding of Indian monsoon dynamics and crop vulnerability in a heat stressed and heavily polluted future India.

Highlights:

1. A rigorous analysis of Aerosol-EF-VPD coupling using collocated direct observations is presented
2. Increased aerosol loading enhances Evaporative Fraction by decreasing sensible heat and increasing latent heat.
3. Aerosols modulate the response of vegetation to changes in VPD under heatwave conditions

Keywords: Grassland, Aerosol loading, eddy covariance, evaporative fraction, physiological response, diffuse radiation, Indo Gangetic Plains, heatwave, sensible heat, latent heat, Bowen ratio

Introduction:

The surface energy balance represents the balance between the net radiation (NR) flux at the Earth's surface and the partitioning of NR into latent heat (LH), sensible heat (SH) and ground heat (GH) fluxes [Wang and Dickinson, 2012]**.** While the dominant partitioning of energy as SH enhances the near-surface air temperature, the LH flux cools the surface and increases the moisture content of the boundary layer. Thus, perturbations to the partitioning of the outgoing turbulent energy fluxes from the land surface modify the near surface micrometeorology. One way of representing this partitioning is the evaporative fraction (EF=LH/(SH+LH)), or the proportion of the total available energy (NR-GH) available at the surface released via vegetation evapotranspiration and soil evaporation. Earlier studies have established that the EF can be modulated by a range of factors, including vapor pressure deficit

(VPD), soil moisture, canopy structure, atmospheric composition, solar radiation and stomatal behaviour [Baldocchi, 1997; Wilson et al., 2002].

The variability in VPD, which describes the near surface moisture deficit for a given temperature (difference between the saturated and ambient vapor pressure for atmospheric water) is arguably the dominant nonlinear forcing on EF variability [Gu et al., 2006]. On one hand, an increase in VPD leads to the partitioning of more of the available energy into LH to meet the atmospheric moisture demand, part of the physical control on evapotranspiration [Penman, 1948; Monteith et al., 1965]. On the other hand, high VPD also triggers partial closure of leaf stomata in response to increased atmospheric dryness [Jones and Sutherland, 1991; Damour et al., 2010; Medlyn et al., 2011]. This is part of the physiological control on ET, causing an increase in VPD to actually decrease ET (and thus EF) [Rigden & Salvucci, 2017]. Moreover, the sign of VPD-EF association could also change due to variations in confounding factors like ambient soil moisture and diffuse/direct radiation [Gu et al., 2006]. More diffused radiation enhances plant productivity [Mercado et al., 2009; Rap et al., 2018] and plant growth [Wang et al., 2018]; which, in turn, can increase LH and EF [Chakraborty et al., 2021;Davin et al., 2012; Wang et al., 2008]. However, this association is also reported to have an optimum point beyond which plant productivity declines with increasing diffused fraction of radiation [Knohl et al., 2008].

Small particles suspended in the atmosphere, i.e. atmospheric aerosols, can alter the amount of shortwave and longwave radiation reaching the surface, through scattering and absorption, thereby altering NR [Schwartz, 1996; Trenberth et al., 2009; Chakraborty and Lee, 2019]. This is commonly known as the aerosol direct radiative effect (ADRE) and is dependent on aerosol size, composition and vertical distribution in the atmosphere [Forster et al., 2007; Sarangi et al., 2016]. Global and regional scale modelling studies have reported that the ADRE can greatly alter the surface fluxes and microclimate over land [Liu et al., 2014; Mallet et al., 2009; Shen et al., 2020; Myhre et al., 2018]. Generally, the ADRE reduces NR, which results in the reduction in the magnitude of SH and LH. But, loading of scattering aerosols from fossil fuel combustion can also increases the diffuse fraction of solar radiation at the surface, which affects the photosynthesis and LH or EF [Chameides et al., 1999; Matsui et al., 2008;Niyogi et al., 2004; Wang et al., 2008; O'Sullivan et al., 2016; Wang et al., 2020]. This mechanism is generally referred to as the diffuse radiation induced aerosol fertilization effect (ADFE). But, depending on the ecosystem, the positive association of ADFE on EF also gets saturated as ADRE becomes larger than a threshold [Yue et al., 2017]. Further, Steiner et al., [2013] reported that warmer air temperature are consistent with high aerosol optical depth (AOD) scenario over various in-situ micrometeorological sites in USA, which can result in no clear association between AOD and LH. Thus, how aerosol loading modulates the already complex VPD-EF association can depend on the interplay between radiation, ADFE, aerosol amount and properties, background climate and ecosystem phenology [Steiner et al., 2011].

Northern India is a global hot spot for atmospheric aerosols with AOD varying between 0.5 and 1.5, and high aerosol radiative efficiency values (~100 W/m^2/AOD) during pre-monsoon period [Dey et al., 2011; Kumar et al., 2015; Dimitris et al., 2012; Sarangi et al., 2016; Srivastava et al., 2011]. In addition, the region also experiences frequent high temperature days and heatwave conditions, generally extending for 2-6 days during this period [Ratnam et al., 2016; Rohini et al., 2016]. During heatwave conditions, the regional atmosphere is largely stagnant [Ratnam et al., 2016], which can lead to greater air temperature by 5-10 K and magnifies the water vapour demand by 2-3 times at weekly time scale. In addition to high air temperatures (T_{air}), high aerosol loading during heatwaves have also been reported over Northern India [Dave et al., 2020; Mondal et al., 2020] at this time of year. Moreover, the value of EF is typically greater than 0.5 over the Northern India during pre-monsoon period, indicating a potentially larger control of VPD-LH linkages on surface energy partitioning [Bhat et al., 2019]. Steep variability in ambient values of VPD (also AOD in some events) during heatwaves over Northern India provides us with ideal conditions for investigating the associations between aerosol loading and VPD-EF coupling.

Previous studies have suggested that aerosol loading can modulate the partitioning of surface fluxes over Northern India [Urankar et al., 2012; Murthy et al., 2014; Latha et al., 2019; Gupta et al., 2020]. However, these studies have been based on reanalysis products [Urankar et al 2012], very limited measurements of SH only [Murthy et al., 2014] or estimated derived from remotely sensed data [Latha et al., 2019] and therefore lack the fidelity that can be obtained from direct observations of key processes. Better understanding of the aerosol-VPD-EF associations using direct collocated observations is essential to understand present day conditions and potential feedbacks that can modify future climate over this region of great hydro-climatic significance. In this study, we have used co-located observations of surface energy balance, near-surface micrometeorological variables and soil characteristics, together with aerosol properties (both surface and columnar) at a sub-tropical site in northern India during the pre-monsoon season. Analysis of case studies with AOD varying in phase or remaining constant with high VPD (under heatwave conditions) are done to understand the underlying processes. Here, we will present compelling evidence that changes in EF is directly (indirectly) proportional to aerosol loading (VPD). More interestingly, we found that aerosol loading can decouple the observed strong VPD-LH relationship under heatwave scenario which can have serious implications on climate resilience of crops and vegetation. Below, the sections are organized to discuss the data used, case studies selected and methodology, results, discussions and summary of this study.

2. Observation site and data:

Observations of SH, LH and net ecosystem CO_2 exchange (NEE) were obtained over a semi-natural grassland site (Figure 1A) within the campus of the Indian Institute of Technology, Kanpur (IITK; 26.5N, 80.3E, elevation 132 m above mean sea level) during the pre-monsoon months (April-June) of 2016-2017. Energy flux data were collected by an eddy covariance system installed at 5.28 m above the soil surface. This flux measurement site is part of an eddy covariance network set up in India as part of the INCOMPASS project of the Indo-UK Monsoon Programme [Chakraborty et al., 2019; Turner et al. 2019; Bhat et al., 2019]. The eddy covariance system consists of a Windmaster sonic anemometer-thermometer (Gill Instruments Ltd. Lymington, UK) and a LI7500 infrared gas analyzer (LI-COR Biosciences, Logan, Utah, USA). The fetch around the tower is a mixture of different C4 grasses, i.e. variants of Napier grass (~60-70%) and some common reed (Scientific family: Pennisetum purpureum and Phragmites-Saccharum-Imperata). Napier grasses are invasive and a perennial species and representative of grasslands in the region (Chakraborty et al., 2019; Holm et al., 1979). The vegetation cover is more than 90% of the fetch of the flux tower (Figure 1B) and the canopy height varied within 1-1.5 m during our study periods. The soil is typical of the Gangetic Plains with silt, clay and sand fractions of 80%, 15% and 5%, respectively (unpublished data). The site experiences a humid subtropical climate. The range in daily AOD and T_{air} was 0.4-1.4 and 32-45 ^{O}C, respectively, during the study period (Figure 1C).

The net radiation (NR; W m^{-2}) and its incoming and outgoing short- and longwave components were measured using an NR01 net radiometer (Hukesflux, Delft, The Netherlands) installed at 5 m above the surface. The surface temperature (T_{srf}) was calculated from the measured outgoing longwave radiation following the Stefan–Boltzmann law assuming an emissivity of 0.95 [Trenberth et al., 2009]. Ground heat fluxes (GH; W m^{-2}) were monitored at 0.03 m below the soil surface using two HFP01-SC self-calibrating soil heat flux plates (Hukesflux, Delft, The Netherlands). Near surface air temperature (T_{air}; ^{o}C) and relative humidity (RH; %) were measured at a height of 4.5 m. Wind speed and wind direction were measured at 10 m above the soil surface using a WindSonic anemometer (Gill Instruments Ltd., Lymington, UK). Volumetric soil water content (VWC; m^3 of water in m^3 of soil) and surface temperature (T_{srf}; ^{o}C) were measured using two pairs of digital TDT sensors (Acclima Inc., Meridian, Idaho, USA) installed at 0.05 and 0.15 m below the soil surface. Standard data processing and quality control routines were used to calculate surface fluxes as described in Morrison et al. 2019. Data gap-filling and the partitioning of net ecosystem exchange into Gross Primary Production (GPP) and total ecosystem respiration was performed using the R EddyProc package [Reichstein et al., 2016; Reichstein et al., 2005]. Negative net ecosystem exchange during the daytime period indicates that photosynthesis at our site dominates over soil and plant respiration (not shown). Since water and carbon cycles in the plants are closely coupled [Collatz et al., 1991]; variations in GPP are used as a proxy for plant transpiration in this study. More details on the flux, weather and radiation tower measurements at IIT Kanpur can be found in Table S1 and Chakraborty et al., 2019.

Version 2 instantaneous cloud screened (Level 1.5) half-hourly averages of Aerosol Optical Depth (AOD) at 550 nm and Single Scattering Albedo (SSA), the ratio of scattering efficiency to total extinction efficiency, at 440 nm obtained from the AErosol RObotic NETwork (AERONET) station deployed in the IITK campus (Figure 1A) were used to quantify the aerosol optical properties during our study period. Low and high SSA values indicate dominance of absorbing and scattering aerosols in the column, respectively. Clear-sky short wave (0.25–4μm) radiative transfer calculations, using the Santa Barbara discrete ordinates radiative transfer Atmospheric Radiative Transfer Model (SBDART) [Ricchiazzi et al., 1998], are used to estimate the midday aerosol direct radiative forcing (ADRF) at surface and diffuse radiation reaching the surface ($diffuse_{frac}$). Midday mean AOD and SSA for each day are prescribed to the model. More details on radiative flux calculations using SBDART are mentioned in Supplementary Information file. Finally, micro-pulse lidar backscatter images (Level 1.5) measured at the collocated Micro-Pulse Lidar Network site [Campbell et al., 2002; Welton and Campbell, 2002] are also used in this study, mainly to identify cloudy days. A day is termed as a cloudy day if cloud patches are observed in Lidar profiles for more than 3 hours. More details on the aerosol measurements can be found in supplementary information file.

3. Case studies and methodology:

In order to examine the impact of aerosols or VPD on EF, we need to carefully identify periods where the variability of other confounding factors is negligible. As such, we identified three weeks (marked in Figure 1C) for analysis, where daily variations in all these factors except T_{air} /VPD and AOD is negligible. Figure 1C illustrates the occurrences of cloudy days, rainfall and wildfire-affected periods during pre-monsoon months of 2016 and 2017. We have avoided periods of cloud and rainfall occurrences since that would affect the surface and energy budget much more than the ADFE. The daily mean VWC values are also shown for the period in Figure 1C. However, as shown in Figure 1C, it is rare to have a considerable time interval with only variation in AOD values (and negligible variation in T_{air}/VPD). Eventually, three one-week periods are carefully selected with different combinations of dominant weekly gradients in T_{air} /VPD and AOD and analyzed to gain insights into ambient AOD-VPD-EF association. The first week selected for analysis is between 2nd-9th June, 2016, which had high weekly gradient in AOD but was accompanied by low variation in T_{air}/VPD (hereafter referred as High AOD-Low T_{air} (HALT) case). The second week is during 10th-15th April, 2017, which witnessed large daily increase in aerosol loading as well as T_{air} in phase throughout the week (hereafter referred to as the High AOD-High T_{air} (HAHT) case). We also selected a third week during 10th-15th May, 2017, when high gradient in T_{air} was observed across the week, but negligible weekly gradient in

AOD was present i.e the AOD values had large day to day variability through the week (hereafter referred to as the Low AOD- High T_{air} (LAHT) case). Interestingly, heatwave conditions were prevalent over North India during the HAHT and LAHT weeks, therefore, a wide range of VPD-AOD-EF variation can be sampled. Moreover, since there were no rainfall events during these three weeks, the variation in VWC was minor compared to large daily variations in T_{air} and AOD during our study periods. Further, the variations in the vegetation phenology, wind and boundary layer height are found to be negligible within each of these three weeks. Note that no week with low AOD and low VPD variations was observed during our study period.

The simultaneous midday (1000-1500 LT) variability in AOD, VPD, EF and the other components of the surface radiative balance is analyzed across the HALT and LAHT weeks to understand the impact of strong weekly gradients of AOD and VPD, respectively. Further, we analyse the weekly gradients in the observations during HAHT, and compare and contrast the same with the HALT and LAHT cases to understand the combined effects of AOD and VPD.

Moreover, to examine the impact of aerosol loading on VPD-EF associations under enhanced heat stress, we also calculated the daily midday bulk canopy resistances for both HAHT and LAHT cases by inverting the Penmann-Monteith equation as described below. We used observed values of available energy, VPD, T_{srf} derived from observed LW_{out}, psychrometric constant and slope of vapor pressure curve derived from observed surface pressure and T_{air} respectively, and aerodynamic resistance derived from the observed SH and near-surface temperature gradient.

The aerodynamic resistance to heat transfer (r_a) is calculated from the near-surface temperature gradient and the measured distance between the two (H), given by:

$$r_a = \frac{-\rho Cp\ (Tsrf - Tair)}{H}$$

where T_{srf} is the surface temperature, calculated by inverting the Stefan-Boltzmann law assuming a unit surface emissivity (reasonable for vegetated surfaces), ρ is the air density, and C_p is the specific heat at constant pressure (1.005×10^{-3} MJ kg^{-1} $°C^{-1}$).

Then, the canopy resistance (r_s) is calculated by inverting the Penman-Monteith approximation. Thus:

$$r_s = \frac{\left(\frac{\Delta(Rn - G) + \frac{\rho CpVPD}{r_a}}{LE}\right) - \Delta}{\gamma - 1} r_a$$

where Δ is the slope of the water vapor saturation curve given by:

$$\Delta = \frac{4098[0.6108\exp(\frac{17.27T_a}{T_a + 237.3})]}{(T_a + 237.3)^2}$$

and γ is the psychrometric constant, calculated as:

$$\gamma = \frac{C_p P}{\varepsilon\lambda}$$

where P is atmospheric pressure in kPa, λ is the latent heat of vaporization (2.45 MJ kg^{-1}), and ε is the ratio of the molecular weight of water vapour to dry air (0.622).

4. Results:

During the HALT period, midday AOD values decreased monotonically across the week from ~1.1 on 2^{nd} June, 2016 to ~ 0.6 on 9^{th} June,2 016 (Figure 2A). The corresponding trend in SSA values was negligible, but SSA values are ~0.92 indicating a predominance of scattering aerosols (Figure 2A). Corresponding values of NR at surface increased monotonically by ~50 W/m^2 during the same week (Figure 2D). The enhancement in midday NR with decreasing AOD is strongly driven by the corresponding increase in midday incoming shortwave radiation (ISWR) by ~100 W/m^2 (Figure 2D). In agreement, ADRF values at surface decreased by ~80 W/m^2 and diffuse fraction of incoming radiation increased by ~0.10 with decrease in scattering aerosols from 2^{nd} June to 9^{th} June, 2016 (Figures S1A and S1D). The daily trend in modelled ADRF (and diffused fraction) values are consistent with the daily reduction trend of ISWR during HALT, reinforcing the expectation that negative daily trend in ISWR and NR during HALT was primarily by aerosol-induced radiative changes.

During HAHT, the midday AOD values increased monotonically across the week from ~0.3 on 10th-11th April to ~ 0.8 on 14th-15th April (Figure 2B). Corresponding values of NR and ISWR at surface decreased monotonically by ~100 W/m^2 and ~200 W/m^2, respectively, during the same period (Figure 2E). Similar to HALT, no daily trend was present in SSA values during HAHT and SSA values are ~ 0.9 indicating presence of scattering aerosols (Figure 2B). In agreement, ADRF values at surface decreased across the week (Figure S1B) with highest values on high AOD days (14th-15th April; ~150 W/m^2) compared to those on low AOD (10th-11th April; ~50 W/m^2). At the same time, the diffuse fraction of incoming radiation at the surface (Figures S1E) increased substantially from ~ 0.5 (on 10th April) to ~0.7 on (15th April) during HAHT indicating strong impact of aerosol loading.

In contrast, during LAHT week, the gradient of AOD values from 10th and 15th May, 2017 was relatively minor (Figure 2C). As the increase in AOD through the week was smaller compared to other two cases, corresponding decrease of NR and ISWR values at surface was also smaller in magnitude (~30 W/m^2) during this period (Figure 2F). Correspondingly, negligible trend in ADRF (Figures S1C) at the surface is observed indicating low variation in aerosol radiative effect change during the LAHT week. Moreover, the midday SSA values during LAHT are lower (~0.8) compared to HALT and HAHT cases indicating presence of highly absorbing aerosols in the column (Figure 2C). Accordingly, the ADRF values at surface during LAHT (Figure S1C) were very high, more than double of the same during HALT and HAHT (i.e. ~350 W/m^2). This can be explained by the fact that absorbing aerosols (lower SSA values) were relatively dominant during LAHT compared to the other 2 cases. Moreover, dominance of absorbing aerosols also lead to minor variation in diffused radiation during the week (Figure S1F). To sum up, the impact of aerosol variability (i.e. the gradient in direct radiative effect and diffused fraction modulation) is minor during the week compared to HAHT and HALT weeks.

As aerosol direct radiative effect induces surface cooling, midday T_{srf} values reduced from ~ 35^{o}C during low AOD days to ~30^{o}C during high AOD days across the HALT week (Figure 3A). At the same time, the variability in T_{air} values remain more or less constant during HALT. Therefore, the midday variation of temperature difference between T_{srf} and T_{air} ($\Delta T = T_{srf}$

- T_{air}) is inversely proportionally with aerosol loading for HALT (Figure 3A). Greater the value of ΔT, greater will be the turbulent and convection flux, and greater is the tendency of SH flux release at surface. Consequently, sensible heat fluxes are also inversely proportional to increase in AOD (and aerosol direct effect). With increase (decrease) in ΔT (AOD) values, the corresponding SH values increased linearly from ~60 W/m^2 on 2nd June to ~ 120 W/m^2 on 9th June, 2016 during HALT week (Figure 3D).

By contrast, a distinct and steep increase in midday T_{air} (~10 ^{o}C) is seen during HAHT and LAHT weeks. Correspondingly, the mid-day T_{srf} values are also seen to be increasing in close coupling with the T_{air} values during these two weeks (Figures 3B-C). This coupling is mainly because of the coexisting stagnant scenario under heatwave periods. Nonetheless, ΔT variation is inversely proportional to AOD variation during both the weeks (Figure 3B-C). Because, some portion of the enhancement in midday T_{srf} is compensated by the aerosol-induced surface cooling, steeper AOD trend across the week means greater ΔT magnitude. For instance, as aerosol radiative effect is relatively smaller across the week during LAHT compared to that during HAHT, a relatively larger decrease in daily ΔT (> 2 ^{o}C) is observed during HAHT week (Figure 3B). Consistently, the magnitude of SH also significantly decreased across the week in HAHT and LAHT. Specifically, the midday mean values of SH decreased linearly from ~200 W/m^2 on 10th April (low AOD) to ~ 100 W/m^2 on 15th April, 2017 (high AOD) during HAHT (Figure 3E). During LAHT, the midday mean SH decreased linearly from ~200 W/m^2 on 11th May to ~ 125 W/m^2 on 14-15th May, 2017 (Figure 3F).

The midday latent heat values decreases by ~150 Wm^{-2} from high AOD days to low AOD days during HALT week (Figure 3D). In comparison, the increase in LH values with increase in AOD across the HAHT week from 10th April,2017 to 15th April, 2017 is gradual i.e. ~25 W/m^{-2} (Figure 3E). Specifically, the slope of regression of latent heat against AOD is 70 W/m^2/AOD and 10 W/m^2/AOD for HALT and HAHT cases, respectively (figure not shown). As, VPD values increase steeply in HAHT case (Figure 3H), but no distinct variation in VPD across the week was evident for HALT case (Figure 3G). Examination of corresponding midday values of gross primary production (GPP) flux (Figures 3G-F) also illustrate gradients similar in sign to corresponding latent heat fluxes indicating that the daily variation in LH flux in both the cases is mainly due to associated variation in evapotranspiration. Keeping in mind that the magnitude of AOD variation in both the above cases are similar, the differences in slopes of LH-AOD regression (lower value during HAHT) could be attributed to the simultaneous suppression of evapotranspiration by VPD rise during HAHT week.

VPD-associated decline in GPP and thus LH fluxes is even more clearly observed during LAHT week. A strong negative trend in midday values of latent heat and GPP is observed as the week progressed from low to high VPD during LAHT (Figure 3F and 3I). Quantitatively, the slope of regression of (midday mean) latent heat against T_{air} is +4.1 $W/m^2/^oC$ and -6.6 $W/m^2/ ^oC$ for HAHT and LAHT cases, respectively. Note that the magnitude of VPD variation in both the cases is similar, so the differences in slope of latent heat and T_{air} regression can be attributed to the corresponding differences in aerosol loading. Thus, the magnitude of latent heat or GPP is directly proportional to changes in magnitude of AOD (as seen in HALT), but the same is inversely proportional to variations in T_{air} or VPD (as seen in LAHT), and the net effects can largely compensate each other (as seen in HAHT).

Moreover, the gradient in EF was substantial only in HAHT and HALT where there was substantial variation in AOD across the week. Partitioning of surface energy into latent heat or the latent heat fraction (LHF: Latent heat / Net radiation) decreased and that into sensible heat fraction (SHF: Sensible heat / Net Radiation) increased with increase in AOD across the week during HALT (Figure 3J). As a result, the midday EF distribution decreased with reduction in AOD from ~0.8 on 2nd June to ~0.6 on 9th June during HALT (Figure 3J). On the same line, with increase in AOD across the week during HAHT, EF also increased from ~0.63 on 10th April, 2017 to ~0.78 on 15th April, 2017 (Figure 3K) due to simultaneous decrease and increase in SHF and LHF, respectively. But, in absence of clear aerosol gradient across the week, no substantial variation was observed in EF across the week during LAHT case (Figure 3L). The decrease in sensible heat with VPD enhancement was similar in HAHT and LAHT cases (Figure 3K-L). But, LH release increased (decreased) with VPD during the former (later) case indicating a role of AOD change on VPD-EF association.

Figure 4 illustrates the variation in midday mean canopy resistance during the LAHT and HAHT weeks to various physical and physiological factors that control evapotranspiration, namely moisture demand, available energy, air temperature and the aerodynamic resistance. As expected, the canopy resistance is significantly ($p<0.05$) correlated with VPD although clear differences in the slope is present for the two cases. Specifically, the canopy resistance increases steeply from 400 to 1400 s m^{-1} with increase in VPD from 40 to 70 hPa during LAHT case (Figure 4a). However, the canopy resistance only increases from 400 to 500 with an increase in VPD from 45 to 65 hPa during HAHT case (Figure 4a). Similarly, air temperature during these periods also shows a statistically significant positive relationship with canopy resistance (Figure 4d). However, during both periods, canopy resistance was found to be independent of available energy (Figure 4c) and the aerodynamic resistance (Figure 4d), indicating that the sensitivity of canopy resistance to changes in VPD (or T_{air}) is significantly greater than that for the other variables.

The LAHT case illustrates the frequently reported behaviour of reduction of canopy conductance under increasing VPD due to partial stomata closure as a physiological stress response (Grossiord et al., 2020). Similar responses are also reported in Napier grasses, the native vegetation over our site (Mwendia et al. 2016). Napier grasses can be anisohydric, i.e. water spending under ample water availability (Cardoso et al., 2015). But their behaviour becomes isohydric under high temperature and high water stress (Liang et al., 2017; Mwendia et al. 2014; Purbajanti et al., 2012). During both HAHT and LAHT weeks, soil moisture is very low, hence, the Napier grasses behaves isohydrically under high VPD. The comparison of LAHT and HAHT scatter illustrates that canopy conductance is not strongly affected even under severe VPD rise when aerosol loading also increases in phase. Specifically, the strong gradient of increase in canopy resistance with VPD/ air temperature gets moderated under the high aerosol scenario. Thus, under the presence of high aerosol loading, the isohydric response of Napier grass to temperature rise or the physiological stress under high VPD is decoupled. This can partially explain the aerosol-induced increase in EF (as well as LH and GPP) even under high VPD rise during HAHT.

Further, meteorological co-variability or any significant differences in weekly pattern of other micro-meteorological variables between HAHT and LAHT cases can also contribute to the corresponding differences in AOD-VPD-EF association. A closer look illustrates that minor gradients are present in the meteorological variables (Figure S2), which can have secondary effects on the VPD-EF associations. Nonetheless, the individual or relative contribution of these meteorological variability and aerosols on the observed coupling remains unknown and deserves further attention in future studies with in depth mechanistic modelling.

5. Discussion:

The increase in scattering aerosols increased diffused radiation during HALT; thereby facilitating relatively more photosynthesis and thus more GPP and latent heat release with increase in AOD. At the same time, increase in AOD also decreased the temperature difference between surface and air and constrained sensible heat release, eventually leading to aerosol-mediated increase in EF during HALT. However, previous studies investigating the role of aerosols on surface energy fluxes over India have largely reported that aerosol loading is inversely related to latent heat [Murthy et al., 2014; Latha et al., 2019; Gupta et al., 2020]. Possible explanations for this apparent contradiction are as follows. First, these studies did not explicitly account for the effect of daily meteorology/ VPD/ temperature variability in their analysis which can have confounding effects (as shown here and discussed in Steiner et al., 2013). Second, these studies were not focused on grassland. Murthy et al., 2014 used micrometeorological site data with a forested footprint in Ranchi. At the same time, Latha et al., 2019 performs analysis at 100 km spatial resolution from reanalysis product/Model, which is representative of a composite land use (including cities, forest, cropland and grassland) and thus a mixture of evapotranspiration and ground evaporation. Gupta et al., 2020 used micrometeorological observations within a typical university canopy (buildings, roads and trees) in Mumbai. Note that total LH can decrease due to aerosols and EF can still increase if SH is decreasing more than EF due to reduction in available energy. Nonetheless, our finding of direct proportionality between aerosol loading and latent heat (or photosynthesis) is consistent with previously reported in-situ studies over grasslands sites in USA [Niyogi et al., 2004; Gu et al., 2002; Wang et al., 2008].

In contrast, aerosol loading and heatwave conditions both supressed sensible heat release. Greater aerosol direct radiative effect induces more surface cooling (Chakraborty and Lee, 2019), and hence lower sensible heat fluxes (Yu et al., 2002; Urankar et al., 2012; Steiner et al., 2013), as seen in HALT case. Simultaneously, sensible heat release is also directly proportional to the near surface temperature gradient during Pre-monsoon (Rao et al., 2019), which is clearly seen in LAHT case. In HAHT case, both the effects work in phase to supress release of sensible heat. The reduction of sensible heat per unit change of T_{air} is 8 $W/m^2/^oC$ during LAHT compared to the same being 11 $W/m^2/^oC$ in HAHT case. At the same time, the reduction of sensible heat per unit change of AOD is 135 W/m^2/AOD during LAHT compared to the same being 65 W/m^2/AOD in HALT case. Hence, increase in AOD and T_{air}, both suppress the release of available surface energy via sensible heat and the effect is largely additive. Moreover, the intensity of the AOD-induced sensible heat suppression will be stronger if the aerosols are composed of relatively more absorbing aerosols, specifically black carbon [Myhre et al., 2018]. Because, they not only cools the T_{srf} (Mallet et al., 2009; Pandithurai et al., 2008a; Shen et al., 2020) but also can warm T_{air} (especially under stagnant/heatwave conditions), thereby reducing the near surface temperature gradient and inducing lower tropospheric stability [Dave et al., 2020; Steiner et al., 2013; Myhre et al., 2018].

However, contrary to our results, a recent modelling study over India reports that enhancement of absorbing aerosols are positively associated with increase in sensible heat and air temperature under heatwave scenario [Mondal et al., 2020]. The inherent model biases in the aerosol properties and concentration as well as absence of detailed canopy-atmosphere processes in the model simulations of Mondal et al., 2020 may cause differences in the signature of the AOD-sensible heat feedback. At the same time, the above differences can also be explained by taking into consideration the difference in time-scale of the feedback used in analysis. For example, a robust positive association between morning time black carbon concentrations and mid-day T_{air} is observed by Talukdar et al., 2020. Although, they attributed this association primarily to diurnal evolution of the residual layer mixing, the understanding from our study can also explain a possible pathway. High black carbon loading during morning time can suppress instantaneous sensible heat release (via reduction in the near surface temperature gradient), followed by release of the additional sensible heat amount in the mid-day period under relatively unstable atmosphere (and lower black carbon concentration due to dilution effect). As such, correlations between absorbing aerosols and sensible heat at instantaneous scale can be negative (as seen in HAHT), but correlations or composite analysis at daily or monthly time scale may involve feedbacks which can result in positive associations (as also seen in Mondal et al., 2020).

In addition, our results clearly underline the complexity and non-linearity between aerosol, VPD and EF, and provides observational evidence to the discussions reported in Steiner et al., 2011; 2013. Keeping all other factors relatively constant, increase in scattering aerosols causes a positive AOD-EF association (as seen in HALT). In case of HAHT, as both AOD and VPD increased in phase over the week, VPD-induced reduction in evapotranspiration compensated a major portion of the aerosol fertilization effect resulting in a slight increase in latent heat with increase in AOD. Also note that, combined effect of increase in AOD and T_{air} caused a large suppression in sensible heat fluxes. Thus, EF also increases with AOD under heatwave conditions. However, in absence of significant aerosol variation, the increase in VPD causes a large reduction in evapotranspiration (as seen in LAHT). First, negligible aerosol fertilization effect and second, increase in canopy resistance (via stomatal aperture reduction) under steep rise in VPD values caused large reduction in latent heat across the week during LAHT. High VPD is also linked with greater T_{air} during heatwave scenarios, thereby inducing reduction the near surface temperature gradient and sensible heat during LAHT. Thus, both sensible heat and latent heat release decreased with VPD causing negligible change in EF with VPD. Thus, the VPD-EF coupling is very strong in absence of aerosol loading but weakens under aerosol loading. Along with aerosol fertilization effect, the direct deposition of aerosols as a wax layer on the leaf surface can also contribute to such an effect [Burkhardt., 2010; Burkhardt and Grantz., 2017]. Recently, Grantz *et al*. 2018 used direct observations in glasshouses to illustrate decoupling of stomata conductance (flux-based) from its porosity (higher VPD induces reduction in pore size) under more aerosol scenario. India’s mean temperature is constantly rising [Krishnan et al., 2020]. At the same time, the global mean VPD is increasing with global warming [Yuan et al., 2019] and heatwaves will be more frequent in future India [Mukherjee et al., 2018]. Moreover, anthropogenic emissions over Indian Subcontinent will ensure high AOD values in near future [Kumar et al 2018], thus manifesting a HAHT-like scenario at longer time scales over India. Although, the response of plants and crops to enhancement in VPD in warmer future is uncertain, but aerosol-induced weakening of VPD-EF associations can contribute towards tendency of crops and vegetations becoming less drought/heat-resilient in future.

6. Summary

In summary, simultaneous observations from AERONET and an eddy covariance flux tower equipped with micrometeorological and soil physics sensors were employed to report possible influence of aerosol loading on VPD-Evaporative Fraction associations over a natural C4 grassland site under clear sky conditions in the central Gangetic Plains. The main findings from this study are:

1. Increase in aerosol loading reduces the incoming solar radiation at surface and reduces the gradient between surface temperature and near-surface air temperature. This is associated with the decrease in energy dissipation from surface via sensible heat. At the same time, increase in aerosol loading increases the evapotranspiration efficiency of ecosystem by increasing diffuse radiation. Thus, high aerosol loading favors dissipation of available surface energy via Latent heat flux and therefore increases Evaporative fraction.
2. Increase in surface temperature and VPD during heatwave conditions induce larger canopy resistance and stomata closure, thereby reducing the LH fluxes and EF. Native Plants tend to store more water by transpiring less in high temperature conditions; so GPP (and thus LH) reduces under high temperatures. At the same time, higher air temperature, also reduces the sensible heat partitioning via reduction in near surface temperature gradient. Thus, as the effect of VPD involves reducing both the surface fluxes, the net effect on EF is negligible.
3. The variability in aerosol loading tends to play a significant role in modulating the VPD-EF association under varying VPD/surface temperature. When the changes in VPD and scattering aerosols are in phase, like in case of stagnant heat wave conditions over North India, the VPD-induced reduction in evapotranspiration may be completely compensated. This physiological changes can be due to the aerosol fertilization effect or thick aerosol deposition/coating on leaves. Besides, as both increasing AOD and T_{air} induces suppression in sensible heat partitioning, largely the changes in net EF remains in phase with changes in AOD and VPD.

Nonetheless, a few caveats of this study need to be kept in mind. Our analysis, although driven by fundamental theory of land-atmosphere interactions, is statistical in nature with a relatively small sample size. The cases we analyse here and carefully selected to represent the distinct scenarios as far as realistically possible in this region. Thus, minor influences of meteorological co-variability cannot be totally avoided. As such, the quantitative estimation of various associations may have inherent uncertainties and care should be taken before generalizing. Moreover, as literature on plant physiological responses specific to grass variants found in the Indo-Gangetic Basin region are scare, this study warrants more species-level studies are necessary to isolate the physiological and environmental responses on EF. Nevertheless, the possible AOD-VPD-EF associations discussed here can have substantial implications on future climate of this and similar subtropical regions. Thus, the observational associations provided in this study not only encourages more measurements, detailed in situ experiments and mechanistic modelling of aerosol-vegetation-atmosphere interactions, but also warrants proper representations of aerosol processes and feedbacks in coupled models over India.

Acknowledgement:

SNT gratefully acknowledge the financial support given by the Earth System Science Organization, Ministry of Earth Sciences, Government of India (grant MM/NERC-MoES-03/2014/002) and Newton Fund to conduct this research under Monsoon Mission. CS acknowledges support from MHRD, India under project number SB20210835CEMHRD00850. LMM acknowledges the support of the Natural Environment Research Council (NERC) South AMerican Biomass Burning Analysis (SAMBBA) project grant code NE/J010057/1. The authors would like to thank Dr E. J. Welton, B.N. Holben and staff at NASA GSFC for establishing and quality control of the AERONET and MPLNET site at IIT Kanpur, used in this study.

Data statement:

Surface data used here is available at: https://catalogue.ceh.ac.uk/documents/78c64025-1f8d-431c-bdeb-e69a5877d2ed. Aerosol data used here is available from https://www.iitk.ac.in/ce/aeronet.

References

1. Bollasina, M. A., and Y. Ming (2013), The role of land-surface processes in modulating the Indian monsoon annual cycle, Climate Dynamics, 41(9-10), 2497-2509.
2. Campbell, J. R., D. L. Hlavka, E. J. Welton, C. J. Flynn, D. D. Turner, J. D. Spinhirne, V. S. S. III, and I. H. Hwang (2002), Full-Time, Eye-Safe Cloud and Aerosol Lidar Observation at Atmospheric Radiation Measurement Program Sites: Instruments and Data Processing, Journal of Atmospheric and Oceanic Technology, 19(4), 431-442.
3. Chakraborty, S., U. Saha, and A. Maitra (2015), Relationship of convective precipitation with atmospheric heat flux — A regression approach over an Indian tropical location, Atmospheric Research, 161–162, 116-124.
4. Chameides, W. L., et al. (1999), Case study of the effects of atmospheric aerosols and regional haze on agriculture: An opportunity to enhance crop yields in China through emission controls?, Proceedings of the National Academy of Sciences, 96(24), 13626-13633.
5. Collatz, G. J., J. T. Ball, C. Grivet, and J. A. Berry (1991), Physiological and environmental regulation of stomatal conductance, photosynthesis and transpiration: a model that includes a laminar boundary layer, Agricultural and Forest Meteorology, 54(2), 107-136.
6. Dey, S., and L. Di Girolamo (2011), A decade of change in aerosol properties over the Indian subcontinent, Geophysical Research Letters, 38(14), n/a-n/a.
7. Dimitris, G. K., P. S. Ramesh, G. Ritesh, S. Manish, P. G. Kosmopoulos, and S. N. Tripathi (2012), Variability and trends of aerosol properties over Kanpur, northern India using AERONET data (2001–10), Environmental Research Letters, 7(2), 024003.
8. Forster, P., V. Ramaswamy, P. Artaxo, T. Berntsen, R. Betts, D. W. Fahey, J. Haywood, J. Lean, D. C. Lowe, and G. Myhre (2007), Changes in atmospheric constituents and in radiative forcing. Chapter 2, in Climate Change 2007. The Physical Science Basis, edited.
9. Gautam, R., N. C. Hsu, and K. M. Lau (2010), Premonsoon aerosol characterization and radiative effects over the Indo-Gangetic Plains: Implications for regional climate warming, Journal of Geophysical Research: Atmospheres, 115(D17), n/a-n/a.
10. Gautam, R., et al. (2011), Accumulation of aerosols over the Indo-Gangetic plains and southern slopes of the Himalayas: distribution, properties and radiative effects during the 2009 pre-monsoon season, Atmos. Chem. Phys., 11(24), 12841-12863.
11. Gu, L., T. Meyers, S. G. Pallardy, P. J. Hanson, B. Yang, M. Heuer, K. P. Hosman, J. S. Riggs, D. Sluss, and S. D. Wullschleger (2006), Direct and indirect effects of atmospheric conditions and soil moisture on surface energy partitioning revealed by a prolonged drought at a temperate forest site, Journal of Geophysical Research: Atmospheres, 111(D16), n/a-n/a.
12. Jones, H. G., and R. A. Sutherland (1991), Stomatal control of xylem embolism, Plant, Cell & Environment, 14(6), 607-612.
13. Liu, S., M. Chen, and Q. Zhuang (2014), Aerosol effects on global land surface energy fluxes during 2003–2010, Geophysical Research Letters, 41(22), 7875-7881.

14. Mallet, M., P. Tulet, D. Serça, F. Solmon, O. Dubovik, J. Pelon, V. Pont, and O. Thouron (2009), Impact of dust aerosols on the radiative budget, surface heat fluxes, heating rate profiles and convective activity over West Africa during March 2006, Atmos. Chem. Phys., 9(18), 7143-7160.
15. Matsui, T., A. Beltrán-Przekurat, D. Niyogi, R. A. Pielke, and M. Coughenour (2008), Aerosol light scattering effect on terrestrial plant productivity and energy fluxes over the eastern United States, Journal of Geophysical Research: Atmospheres, 113(D14), n/a-n/a.
16. Murthy, B. S., R. Latha, K. Manoj, and N. C. Mahanti (2014), Effect of aerosols on evapo-transpiration, Atmospheric Environment, 89, 109-118.
17. Niyogi, D., H.-I. Chang, F. Chen, L. Gu, A. Kumar, S. Menon, and R. A. Pielke (2007), Potential impacts of aerosol–land–atmosphere interactions on the Indian monsoonal rainfall characteristics, Natural Hazards, 42(2), 345-359.
18. Niyogi, D., et al. (2004), Direct observations of the effects of aerosol loading on net ecosystem CO2 exchanges over different landscapes, Geophysical Research Letters, 31(20), n/a-n/a.
19. Pandithurai, G., C. Seethala, B. S. Murthy, and P. C. S. Devara (2008a), Investigation of atmospheric boundary layer characteristics for different aerosol absorptions: Case studies using CAPS model, Atmospheric Environment, 42(19), 4755-4768.
20. Pandithurai, G., S. Dipu, K. K. Dani, S. Tiwari, D. S. Bisht, P. C. S. Devara, and R. T. Pinker (2008b), Aerosol radiative forcing during dust events over New Delhi, India, Journal of Geophysical Research: Atmospheres, 113(D13), n/a-n/a.
21. Saha, S. K., S. Halder, K. K. Kumar, and B. N. Goswami (2011), Pre-onset land surface processes and 'internal' interannual variabilities of the Indian summer monsoon, Climate Dynamics, 36(11), 2077-2089.
22. Sarangi, C., S. N. Tripathi, A. K. Mishra, A. Goel, and E. J. Welton (2016), Elevated aerosol layers and their radiative impact over Kanpur during monsoon onset period, Journal of Geophysical Research: Atmospheres, 121(13), 7936-7957.
23. Schwartz, S. E. (1996), Atmospheric AerosolsThe whitehouse effect—Shortwave radiative forcing of climate by anthropogenic aerosols: an overview, Journal of Aerosol Science, 27(3), 359-382.
24. Srivastava, A., S. Tiwari, P. Devara, D. Bisht, M. K. Srivastava, S. Tripathi, P. Goloub, and B. Holben (2011), Pre-monsoon aerosol characteristics over the Indo-Gangetic Basin: implications to climatic impact, paper presented at Annales Geophysicae, European Geosciences Union.
25. Steiner, A. L., and W. L. Chameides (2011), Aerosol-induced thermal effects increase modelled terrestrial photosynthesis and transpiration, Tellus B, 57(5).
26. Steiner, A. L., D. Mermelstein, S. J. Cheng, T. E. Twine, and A. Oliphant (2013), Observed Impact of Atmospheric Aerosols on the Surface Energy Budget, Earth Interactions, 17(14), 1-22.
27. Trenberth, K. E., J. T. Fasullo, and J. Kiehl (2009), Earth's Global Energy Budget, Bulletin of the American Meteorological Society, 90(3), 311-323.
28. Urankar, G., T. V. Prabha, G. Pandithurai, P. Pallavi, D. Achuthavarier, and B. N. Goswami (2012), Aerosol and cloud feedbacks on surface energy balance over selected regions of the Indian subcontinent, Journal of Geophysical Research: Atmospheres, 117(D4), n/a-n/a.

29. Wang, K., and R. E. Dickinson (2012), A review of global terrestrial evapotranspiration: Observation, modeling, climatology, and climatic variability, Reviews of Geophysics, 50(2), n/a-n/a.
30. Wang, K., R. E. Dickinson, and S. Liang (2008), Observational evidence on the effects of clouds and aerosols on net ecosystem exchange and evapotranspiration, Geophysical Research Letters, 35(10), n/a-n/a.
31. Welton, E. J., and J. R. Campbell (2002), Micropulse Lidar Signals: Uncertainty Analysis, Journal of Atmospheric and Oceanic Technology, 19(12), 2089-2094.
32. Yu, H., S. C. Liu, and R. E. Dickinson (2002), Radiative effects of aerosols on the evolution of the atmospheric boundary layer, Journal of Geophysical Research: Atmospheres, 107(D12), AAC 3-1-AAC 3-14.
33. Koster, R. D., Dirmeyer, P. A., Guo, Z., Bonan, G., Chan, E., Cox, P., ... & Liu, P. (2004). Regions of strong coupling between soil moisture and precipitation. *Science*, *305*(5687), 1138-1140.
34. Turner, A. G., Bhat, G. S., Martin, G. M., Parker, D. J., Taylor, C. M., Mitra, A. K., ... & Morrison, R. (2019). Interaction of convective organization with monsoon precipitation, atmosphere, surface and sea: The 2016 INCOMPASS field campaign in India. *Quarterly Journal of the Royal Meteorological Society*.
35. Chakraborty, T., & Lee, X. (2019). Land cover regulates the spatial variability of temperature response to the direct radiative effect of aerosols. *Geophysical Research Letters*, *46*(15), 8995-9003.
36. Chakraborty, T., Sarangi, C., Krishnan, M., Tripathi, S. N., Morrison, R., & Evans, J. (2019). Biases in model-simulated surface energy fluxes during the Indian monsoon onset period. *Boundary-Layer Meteorology*, *170*(2), 323-348.
37. Chakraborty, T. C., Lee, X., & Lawrence, D. M. (2021). Strong local evaporative cooling over land due to atmospheric aerosols. Journal of Advances in Modeling Earth Systems, 13(5), e2021MS002491.

38. Rigden, A. J., & Salvucci, G. D. (2017). Stomatal response to humidity and CO 2 implicated in recent decline in US evaporation. *Global Change Biology*, *23*(3), 1140-1151.
39. Yuan, W., Zheng, Y., Piao, S., Ciais, P., Lombardozzi, D., Wang, Y., ... & Jain, A. K. (2019). Increased atmospheric vapor pressure deficit reduces global vegetation growth. *Science advances*, *5*(8), eaax1396.
40. Wang Z., C. Wang, B. Wang, X. Wang, J. Li, J. Wu, L. Liu Interactive effects of air pollutants and atmospheric moisture stress on aspen growth and photosynthesis along an urban-rural gradient. Environ. Pollut., 260 (2020), Article 114076, 10.1016/j.envpol.2020.114076
41. Burkhardt J, Grantz DA. 2017. Plants and atmospheric aerosols. Progress Botany 78: 369–406
42. Burkhardt J. 2010. Hygroscopic particles on leaves: nutrients or desiccants? *Ecological Monographs* **80**: 369– 399.
43. Grantz DA, Zinsmeister D, Burkhardt J. 2018. Ambient aerosol increases minimum leaf conductance and alters the aperture–flux relationship as stomata respond to vapor pressure deficit (VPD). *New Phytologist* **219**: 275– 286.

44. R. Latha, B. S. Murthy & B. Vinayak (2019) Aerosol-induced perturbation of surface fluxes over different landscapes in a tropical region, International Journal of Remote Sensing, 40:21, 8203-8221, DOI: 10.1080/01431161.2018.1523586
45. Krishnan et al (2020) Assessment of climate change over the Indian region: a report of the Ministry of Earth Sciences (MoES), Government of India
46. WangX., J. Wu, M. Chen, X. Xu, Z. Wang, B. Wang, C. Wang, S. Piao, W. Lin, G. Miao, Deng, C. Qiao, J. Wang, S. Xu, L. Liu, Field evidences for the positive effects of aerosols on tree growth. Global Change Biol., 24 (2018), pp. 4983-4992
47. Myhre, G., Samset, B.H., Hodnebrog, Ø. *et al.* Sensible heat has significantly affected the global hydrological cycle over the historical period. *Nat Commun* **9,** 1922 (2018). https://doi.org/10.1038/s41467-018-04307-4
48. Rao, K. G., & Reddy, N. N. (2019). On moisture flux of the Indian summer monsoon: A new perspective. *Geophysical Research Letters*, 46, 1794– 1804. https://doi.org/10.1029/2018GL080392
49. Mondal, A, Sah, N, Sharma, A, Venkataraman, C, Patil, N. Absorbing aerosols and high-temperature extremes in India: A general circulation modelling study. *Int J Climatology*. 2020; 1– 20. https://doi.org/10.1002/joc.6783
50. Shen Z, Ming Y, Held IM. Using the fast impact of anthropogenic aerosols on regional land temperature to constrain aerosol forcing. Sci Adv. 2020 Aug 5;6(32): doi: 10.1126/sciadv.5297.
51. Dave P, Bhushan, M., Venkatraman, C., Absorbing aerosol influence on temperature maxima: An observation-based study over India. Atmospheric Environment, Volume 223, 2020, 117237, ISSN 1352-2310, https://doi.org/10.1016/j.atmosenv.2019.117237.
52. Talukdar S. and M.V. Ratnam, A mutual response between surface temperature and black carbon mass concentration during the daytime, Science of the Total Environment, https://doi.org/10.1016/j.scitotenv.2020.143477
53. Knohl, A., and D. D. Baldocchi (2008), Effects of diffuse radiation on canopy gas exchange processes in a forestecosystem, J. Geophys. Res., 113, G02023, doi:10.1029/2007JG000663
54. Davin, E. L. and Seneviratne, S. I.: Role of land surface processes and diffuse/direct radiation partitioning in simulating the European climate, Biogeosciences, 9, 1695–1707, https://doi.org/10.5194/bg-9-1695-2012, 2012
55. O’Sullivan, M., A. Rap, C. L. Reddington,D. V. Spracklen, M. Gloor, andW. Buermann (2016), Small global effecton terrestrial net primary productiondue to increased fossil fuel aerosol emissions from East Asia since the turnof the century, Geophys. Res. Lett., 43,8060–8067, doi:10.1002/2016GL068965.
56. Yue, X. and Unger, N.: Aerosol optical depth thresholds as a tool to assess diffuse radiation fertilization of the land carbon uptake in China, Atmos. Chem. Phys., 17, 1329–1342, https://doi.org/10.5194/acp-17-1329-2017, 2017.
57. Mercado LM, Bellouin N, Sitch S, Boucher O, Huntingford C, Wild M, Cox PM. Impact of changes in diffuse radiation on the global land carbon sink. Nature. 2009 Apr 23;458(7241):1014-7. doi: 10.1038/nature07949. PMID: 19396143.
58. Kumar, R., Barth, M. C., Pfister, G. G., Delle Monache, L., Lamarque, J. F., Archer-Nicholls, S.,Walters, S. (2018). How will air quality change in South Asia by 2050? *Journal of Geophysical Research: Atmospheres*, 123, 1840– 1864. https://doi.org/10.1002/2017JD027357

59. M. Kumar, K.S. Parmar, D.B. Kumar, A.Mhawish, D.M. Broday, R.K. Mall, T. Banerjee Long-term aerosol climatology over Indo-Gangetic Plain: trend, prediction and potential source field; Atmos. Environ., 180 (2018), pp. 37-50
60. Bhat G. S., R. Morrison, C. M. Taylor, B. K. Bhattacharya, S. Paler,D. Desai,J. G. Evans,S. Pattnaik, M. Sekhar, R. Nigam, A. Sattar, S. S. Angadi, D. Kacha, A. Patidar, S. N. Tripathi, K. V. M. Krishnan, A. Sisodiya; Spatial and temporal variability in energy and water vapour fluxes observed at seven sites on the Indian subcontinent during 2017. *Q J R Meteorol Soc*. 2020; 146: 2853– 2866. https://doi.org/10.1002/qj.3688
61. Ratnam, J., Behera, S., Ratna, S. *et al.* Anatomy of Indian heatwaves. *Sci Rep* 6, 24395 (2016). https://doi.org/10.1038/srep24395.
62. Mukherjee, S., Mishra, V. A sixfold rise in concurrent day and night-time heatwaves in India under 2 °C warming. *Sci Rep* **8,** 16922 (2018). https://doi.org/10.1038/s41598-018-35348-w
63. Morrison, R.; Angadi, S.S.; Cooper, H.M.; Evans, J.G.; Rees, G.; Sekhar, M.; Taylor, C.; Tripathi, S.N.; Turner, A.G. (2019). Energy and carbon dioxide fluxes, meteorology and soil physics observed at INCOMPASS land surface stations in India, 2016 to 2017. NERC Environmental Information Data Centre. https://doi.org/10.5285/78c64025-1f8d-431c-bdeb-e69a5877d2ed
64. Mayank Gupta et al 2021 Environ. Res. Lett. 16 014021
65. Rohini, P., Rajeevan, M. & Srivastava, A. On the Variability and Increasing Trends of Heat Waves over India. *Sci Rep* **6,** 26153 (2016). https://doi.org/10.1038/srep26153
66. Mwendia, S. W., Yunusa, I. A., Sindel, B. M., Whalley, R. D., & Kariuki, I. W. (2017). Assessment of Napier grass accessions in lowland and highland tropical environments of East Africa: water stress indices, water use and water use efficiency. *Journal of the Science of Food and Agriculture*, *97*(6), 1953-1961.
67. van Heerwaarden, C. C., & Teuling, A. J. (2014). Disentangling the response of forest and grassland energy exchange to heatwaves under idealized land–atmosphere coupling. *Biogeosciences*, *11*(21), 6159-6171.
68. Juan Andrés Cardoso, Marcela Pineda, Juan de la Cruz Jiménez, Manuel Fernando Vergara, Idupulapati M. Rao, Contrasting strategies to cope with drought conditions by two tropical forage C_4grasses, *AoB PLANTS*, Volume 7, 2015, plv107, https://doi.org/10.1093/aobpla/plv107
69. Liang, X., Erickson, J.E., Sollenberger, L.E., Rowland, D.L., Silveira, M.L. and Vermerris, W. (2018), Growth and Transpiration Responses of Elephantgrass and Energycane to Soil Drying. Crop Science, 58: 354-363. https://doi.org/10.2135/cropsci2017.01.0019
70. Purbajanti, E.; Anwar, S.; Wydiati, F.K. Drought stress effect on morphology characters, water use efficiency, growth and yield of guinea and napier grasses. *Int. Res. J. Plant Sci.* **2012**, *3*, 47. [**Google Scholar**]
71. Mwendia, S.; Yunusa, I.; Whalley, R.; Sindel, B.; Kenney, D.; Kariuki, I. Use of plant water relations to assess forage quality and growth for two cultivars of Napier grass (*Pennisetum purpureum*) subjected to different levels of soil water supply and temperature regimes. *Crop Pasture Sci.* **2014**, *64*, 1008–1019. [**Google Scholar**]
72. Holm L, Pancho JV, Herberger JP, Plucknett DL, 1979. A Geographical Atlas of World Weeds. Toronto, Canada: John Wiley and Sons Inc

73. Charlotte Grossiord, Thomas N. Buckley, Lucas A. Cernusak, Kimberly A. Novick, Benjamin Poulter, Rolf T. W. Siegwolf, John S. Sperry, Nate G. McDowell
74. Irmak, S., and Mutiibwa, D. (2010), On the dynamics of canopy resistance: Generalized linear estimation and relationships with primary micrometeorological variables, *Water Resour. Res.*, 46, W08526, doi:10.1029/2009WR008484.

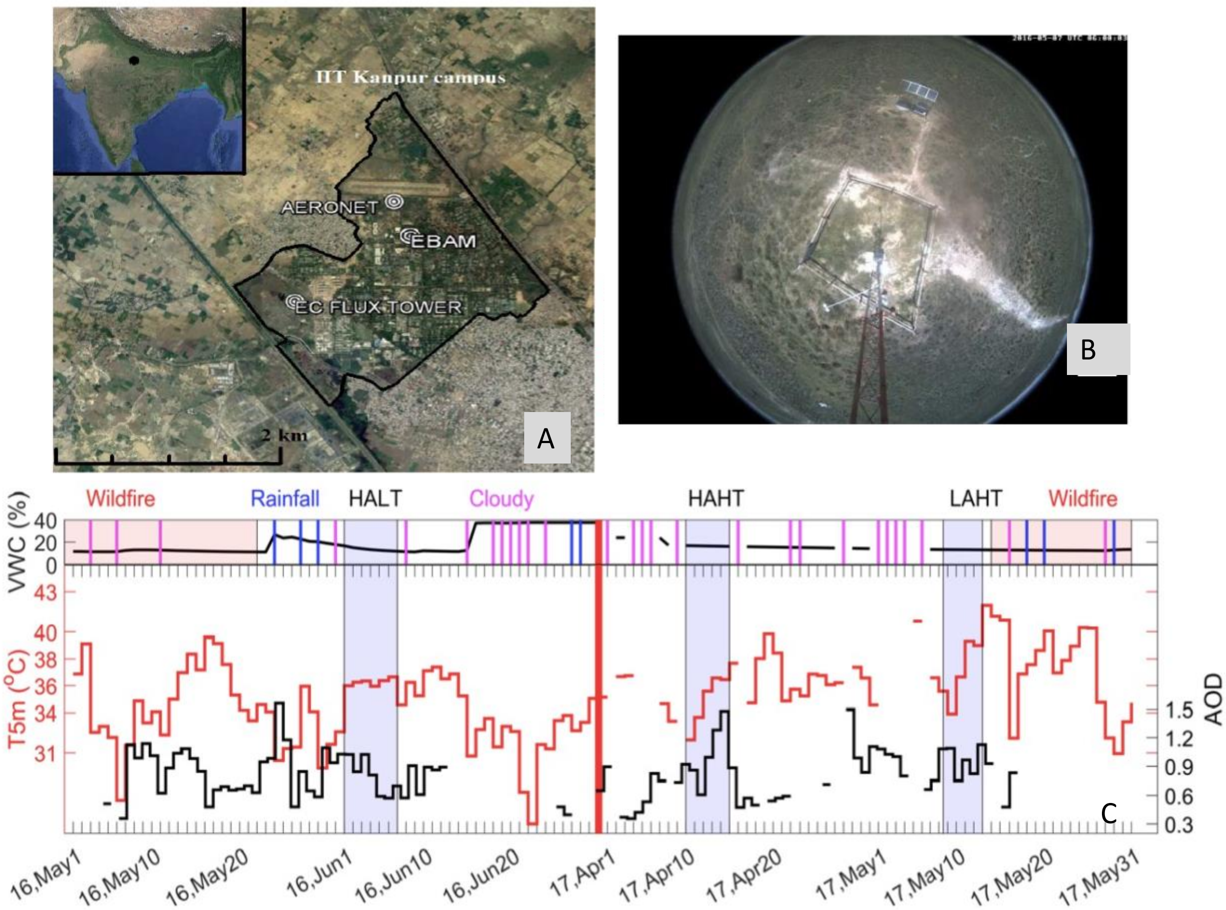

Figure 1: A) Map showing the locations of AERONET and the EC flux tower site within the campus of the Indian Institute of Technology Kanpur (IITK). Inset map shows the location of IITK (black dot) in the central Gangetic Plains. The maps are created by © Google Maps 2017. B) Camera image of land cover of the flux tower site during May 12th, 2017. C) Daily variation in soil moisture (VWC, volumetric water content) during our study period is shown in black line in upper box of the figure. The occurrences of cloudy days, rainy days and wildfire affected period during April through June of 2016 and 2017 is shown by magenta, blue and pink colour patches in the upper box. A cloudy day is inferred from MPLNET images and AERONET observations (as defined in Section 2 of main text). The days bounded by straight lines depict the weekly episodes HALT, HAHT and LAHT, respectively. Daily variation in T_{air} and daily variation in AOD during our study period is shown as black and red lines in lower box of the panel.

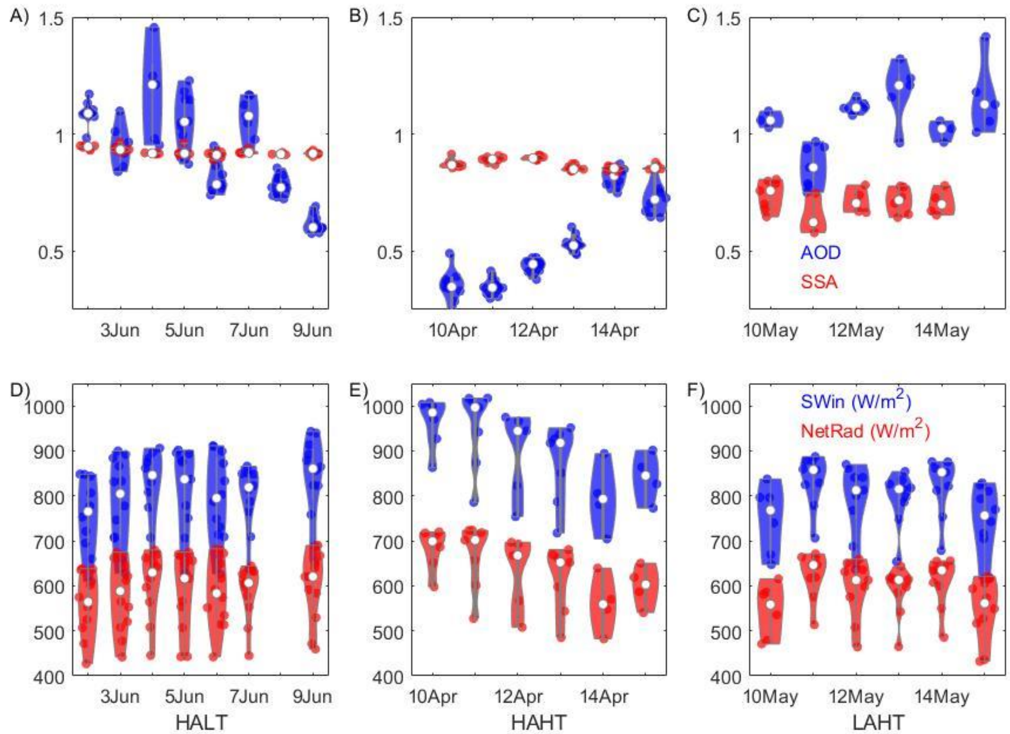

Figure 2: Distribution plots showing the variations in aerosol and radiation during the cases. Row 1 illustrates Time series of midday (1100-1400 LT) variation in AOD and SSA values during HALT, HAHT and LAHT, respectively.. The horizontal line within box represents median of the distribution. The bottom and top edge of the boxes represent 25th and 75th percentile, respectively, of the distribution. The short dash at top and bottom extent of the boxes represent 5th and 95th percentile, respectively. Row 2 is same as Row 1 but show measurements of incoming short wave radiation and net radiation at surface. Note that June,16 means June of 2016 and so on.

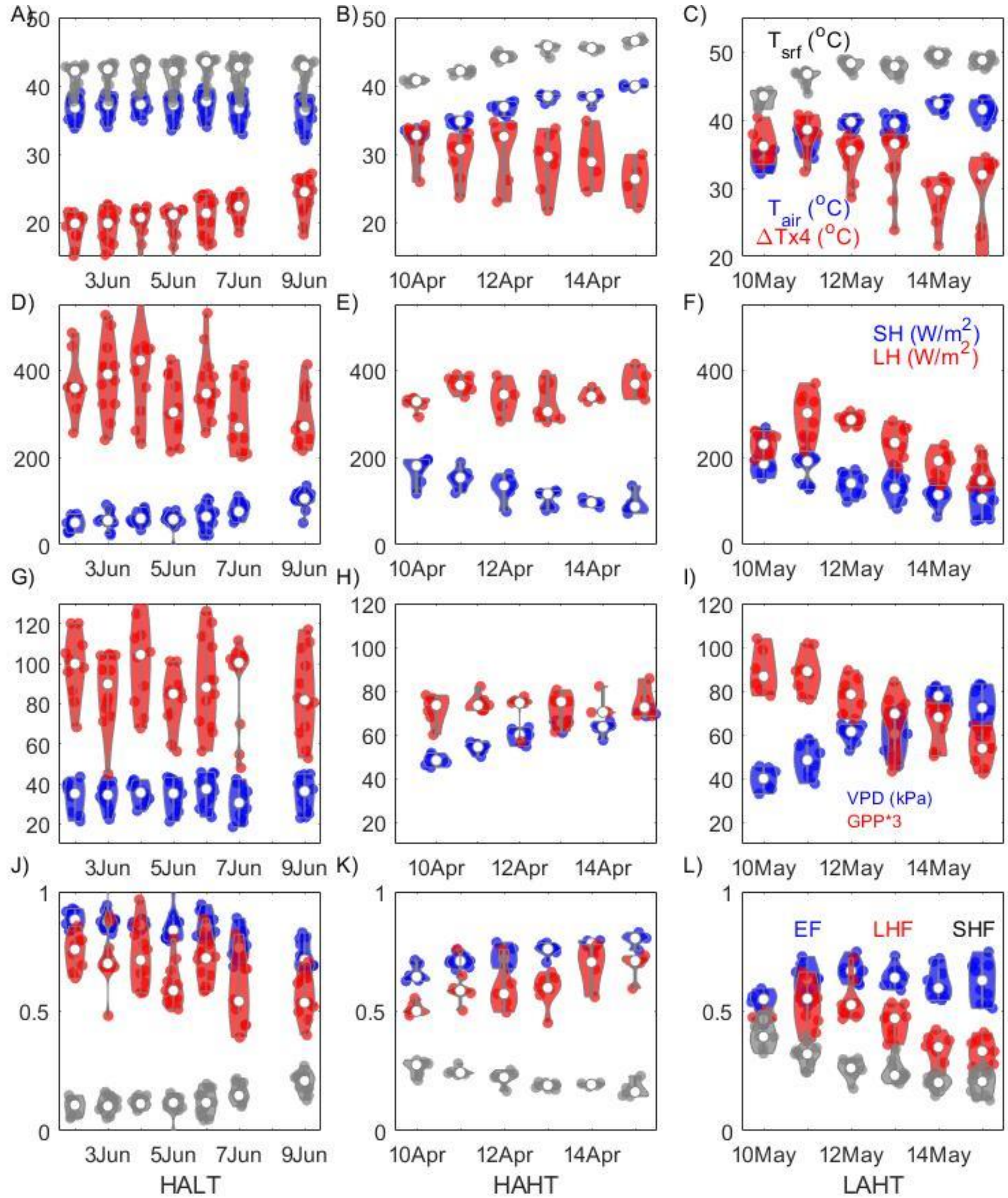

Figure 3: Distribution plots showing the variations in near surface meteorology and surface fluxes during the cases. Row 1 illustrates Time series of midday (1100-1400 LT) variation in T_{srf}, T_{air} and (-)ΔT values during HALT, HAHT and LAHT, respectively. Row 2 is same as Row 1 but for SH and LH. Row 3 is same but for VPD and GPP ; Row 4 is same but for EF, LHF (red) and SHF.

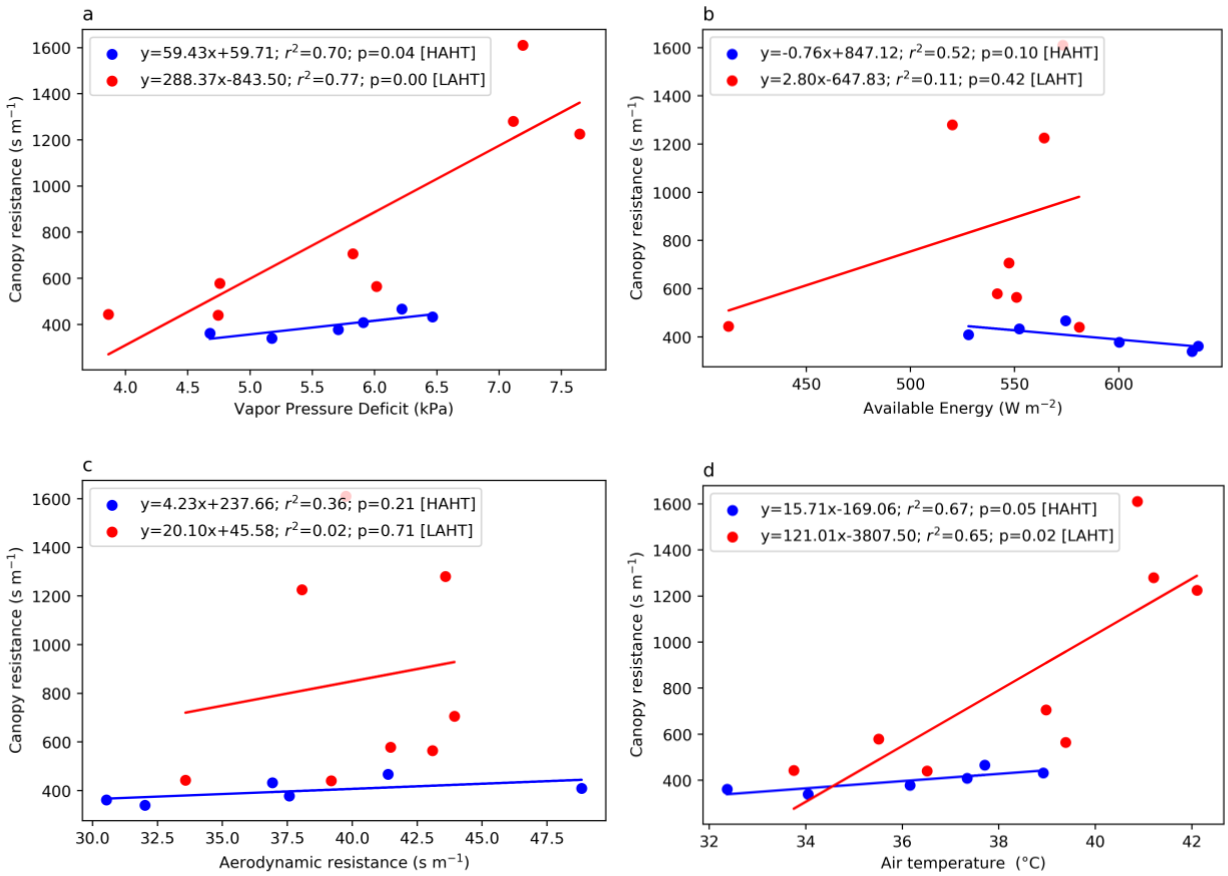

Figure 4: Linear correlation between daily midday average Canopy resistance derived from Penman-Monteith equation with a) observed Vapor Pressure Deficit (VPD); b) Available energy at surface; c) Aerodynamic resistance and d) Air temperature for HAHT and LAHT cases.

Appendix A: Table of Abbreviations

Name	Abrv. used
Latent heat flux	LH
Sensible heat flux	SH
Ground heat flux	GH
Evaporative Fraction	EF
2 m air temperature	T_{air}
vapor pressure deficit	VPD
gross primary production	GPP
net radiation	NR
aerosol direct radiative effect	ADRE
aerosol diffuse radiation fertilization effect	ADFE
diffuse radiation	$diffuse_{frac}$
Santa Barbara discrete ordinates radiative transfer Atmospheric Radiative Transfer Model	SBDART
AErosol RObotic NETwork	AERONET
Volumetric soil water content	VWC
surface temperature	T_{srf}
relative humidity	RH
Aerosol Optical Depth	AOD
Single Scattering Albedo	SSA
High AOD-Low T_{air}	HALT
High AOD-High T_{air}	HAHT
Low AOD- High T_{air}	LAHT
Outgoing long wave radiation at surface	LW_{out}
canopy resistance	r_s
aerodynamic resistance to heat transfer	r_a
Sensible heat fraction	SHF
Latent heat fraction	LHF